3rd AIAA Flow Control Conference, 5–8 June 2006, San Francisco

# Reduced-Order Modeling of Channel Flow Using Traveling POD and Balanced POD

M. Ilak and C. W. Rowley

*Dept. of Mechanical and Aerospace Engineering, Princeton University, Princeton, NJ 08544*

**Reduced-order models of the flow in a plane channel flow are constructed in two regimes: a minimal flow unit in which turbulence is sustained, and a transitional flow linearized about the laminar profile. Proper orthogonal decomposition (POD) of data from a direct numerical simulation of a channel flow in a minimal flow unit is performed in order to examine the coherent structures and their dynamical interactions. Empirical basis functions are obtained both using Fourier modes in the streamwise and spanwise directions, with POD modes in the wall-normal direction, and using 3D (non-Fourier) POD modes that can translate in the streamwise direction (traveling modes). Traveling modes capture more energy than standard Fourier-POD for the same number of modes. In addition, models of a channel flow linearized about a laminar profile are constructed using both POD and balanced POD, an approximation to balanced truncation that is tractable for very large systems. Balanced POD models significantly outperform standard POD, especially at including the effects of actuation.**

## I. Introduction

Seeking low-dimensional models of turbulent flows is motivated both by the desire to describe and understand turbulence on a fundamental level using the tools of dynamical systems theory, and the potential for a wide range of applications in flow control. The standard method of obtaining low-dimensional models is Galerkin projection, where the Navier-Stokes equations are projected onto a low-dimensional subspace, which is often obtained through proper orthogonal decomposition (POD).[1–4] Various improvements have been made in recent years, including the use of shift modes,[5,6] improved representations of the pressure term,[7] methods for compressible flows,[8] and the use of traveling POD modes.[9]

In this paper, we investigate the feasibility and performance of low-order models for two important regimes of channel flow. First, we compare the traveling POD procedure to the standard POD procedure for the turbulent flow in a minimal flow unit channel, the smallest domain of simulation where turbulent structures can be sustained,[4,10] where it is expected that the dynamical behavior of the flow is as simple as possible for a turbulent flow. Although the MFU is an idealization rather than a practically realizable flow, its modeling is expected to provide the basis for further understanding of turbulence on larger domains with more complicated dynamical behavior. Next, we consider the case of transitional flow, where the governing equations are still linear, and form reduced-order models using standard POD and balanced POD, an alternative method proposed recently.[11] This method has the advantage of capturing the dynamics of the flow, with the potential for application in closed-loop flow control, and with the possibility of extension to non-linear systems.

## II. Traveling POD in a Minimal Unit Channel

### A. Traveling POD

The expansion of the velocity field as a sum of POD modes is given by

$$\mathbf{u}(x,y,z,t) = \sum_{j=1}^{n} a_j(t)\boldsymbol{\varphi}_j(x,y,z) \tag{1}$$

where $\boldsymbol{\varphi}_j(x,y,z)$ are the modes and $a_j(t)$ their corresponding time coefficients. For problems that are invariant in one or more spatial dimensions, if one wishes to preserve this symmetry in the reduced-order subspace, the optimal modes are Fourier modes in the spatially invariant directions.[2,3] Our problem is invariant in both streamwise and spanwise directions, so the modes $\boldsymbol{\varphi}_j$ are Fourier modes in these directions, and POD modes in the wall-normal direction, given by

$$\mathbf{u}(x,y,z,t) = \frac{1}{\sqrt{L_x L_z}} \sum_j \sum_{n_x} \sum_{n_z} a^{(j)}_{n_x,n_z}(t) \exp\left(2\pi i \left(\frac{n_x x}{L_x} + \frac{n_z z}{L_z}\right)\right) \phi^{(j)}_{n_x,n_z}(y) \tag{2}$$

as used by Moin and Moser[12] for channel flow and Smith[4] for Couette flow. The theory of this method can be found in these references. We shall further refer to the modes $\phi^{(j)}_{n_x,n_z}$ as 'Fourier POD modes.' The Fourier POD modes are one-dimensional, and the triple sum is over all $(x,z)$ wavenumber pairs as well as over all modes corresponding to each pair. $L_x$ and $L_z$ are the streamwise and spanwise domain sizes respectively.

An alternative way to retain the property of translation invariance is by using traveling POD modes, so that the dynamics of turbulent structures can be observed from the point of view of an observer moving with the flow, expanding the velocity field as

$$\mathbf{u}(x,y,z,t) = \sum_{j=1}^{n} a_j(t)\boldsymbol{\varphi}_j(x-c(t),y,z) \tag{3}$$

The value of the shift $c(t)$ may be determined by shifting the solution to line up best with a preselected template function. A detailed description of the method is given in Rowley and Marsden,[9] which also gives a method for reconstructing the shift $c(t)$ in reduced-order models. In traveling POD, the first velocity snapshot is used as the template for the second one, the shifted second snapshot is the template for fitting the third one, etc. (This method has been called the *method of connections*.[9]) In our calculations, the shifting is performed in the Fourier domain.

### B. Numerical simulation and POD mode calculation

Direct Numerical Simulations (DNS) were performed using the spectral collocation method described by Kim et al.,[13] with periodic boundary conditions in the streamwise and spanwise directions. The simulation parameters chosen were those given by Jimenez and Moin[10] for a minimal unit at centerline Reynolds number $Re = 3000$, with the corresponding $Re_\tau = 130$. The grid resolution was $32 \times 128 \times 16$, and the domain size in streamwise and spanwise directions was $\pi \times 0.3\pi$. The simulation was started using a converged velocity profile for a larger domain. The convergence of the simulation was validated by computing the r.m.s. velocity fluctuations $\langle uu\rangle^{\frac{1}{2}}$,$\langle vv\rangle^{\frac{1}{2}}$ and $\langle ww\rangle^{\frac{1}{2}}$, the total stress and Reynolds stresses $-\langle uv\rangle^{\frac{1}{2}}$ and by plotting the velocity in terms of the inner coordinate $y^+$ and comparing it to the linear law in the inner region and the logarithmic law in the outer region. The velocity fluctuations and the mean velocity profile matched well those given in Jimenez and Moin.[10]

The POD modes can be computed using two methods: the direct method, which involves the solution of an $n \times n$ eigenvalue problem, where $n$ is three times the the number of grid points in the simulation (for three velocity components); or the *method of snapshots*, which involves the solution of an $m \times m$ eigenvalue problem, where $m$ is the number of "snapshots" of the flow taken for the calculation.[3] The direct method is often intractable for the grid sizes used in DNS, and the method of snapshots is faster. However, for the Fourier modes, POD was performed only in the wall-normal direction at each $(n_x, n_z)$ wavenumber pair, the direct method was less computationally expensive for the number of snapshots used. Before taking the POD, the data set is extended by symmetrization. This takes into account the three discrete symmetries in

channel flow: reflection in the wall-normal and spanwise directions, and rotation about the streamwise ($x$) axis.[3]

The POD was performed on three sets which included approximately 80 flow-through times of the channel each. For both the Fourier modes and the traveling modes, the mean streamwise velocity (over space and time) for the whole DNS data set was subtracted from the data before taking the POD, as we are interested in the velocity fluctuations only. In runs where this was not done, the mean profile was obtained as the most significant mode by the POD calculation, with the same energy budget for the remaining modes.

### C. Comparison of the two methods

**Table 1. Comparison of the energy budget for Fourier modes among three data sets**

| | Dataset 1 | | | Dataset 2 | | | Dataset 3 | | |
|---|---|---|---|---|---|---|---|---|---|
| 'rank' | $n_x, n_x, n$ | $\lambda/E_1$, Fourier | $\lambda/E_1$, traveling | $n_x, n_x, n$ | $\lambda/E_2$, Fourier | $\lambda/E_2$, traveling | $n_x, n_x, n$ | $\lambda/E_3$, Fourier | $\lambda/E_3$, traveling |
| 1 | $0, \pm1, 1$ | 0.132 | 0.090 | $0, \pm1, 1$ | 0.147 | 0.084 | $0, \pm1, 1$ | 0.134 | 0.088 |
| 2 | $0, \pm1, 2$ | 0.111 | 0.077 | $0, \pm1, 2$ | 0.117 | 0.073 | $0, \pm1, 2$ | 0.105 | 0.064 |
| 3 | $\pm1, \pm1, 1$ | 0.051 | 0.067 | $\pm1, \pm1, 1$ | 0.058 | 0.073 | $\pm1, \pm1, 1$ | 0.066 | 0.062 |
| 4 | $\pm1, \pm1, 2$ | 0.048 | 0.037 | $\pm1, \pm1, 2$ | 0.041 | 0.057 | $\pm1, \pm1, 2$ | 0.041 | 0.059 |
| 5 | $0, \pm1, 3$ | 0.024 | 0.024 | $\pm1, 0, 1$ | 0.023 | 0.025 | $\pm1, 0, 1$ | 0.031 | 0.027 |
| total | | 0.366 | 0.295 | | 0.386 | 0.311 | | 0.377 | 0.302 |
| 14 modes | | | 0.453 | | | 0.469 | | | 0.465 |

Table 1 shows a comparison of the first several most significant traveling and Fourier modes, for three different time intervals of the same length selected out of a DNS run. These modes were computed for the whole channel. It should be noted that for non-zero streamwise and spanwise wavenumbers, the Fourier modes come in pairs or groups of four, with equal eigenvalues (due to the reality condition). Thus, in Table 1 we are actually comparing 14 Fourier modes with five traveling modes. The fraction of energy included in the first 14 traveling modes, which would correspond to a dynamical system of same dimension as the one obtained using the Fourier modes, is also shown in Table 1, and is on average 22.9% higher than that of the first 14 Fourier modes.

Although the Fourier modes are related via the reality condition

$$a^{(n)}_{n_x,n_z}(t) = a^{(n)*}_{-n_x,-n_z} \tag{4}$$

they are still complex, and the order of a system describing the flow using Fourier modes would be at least twice the order of the system described using traveling modes, unless modes with $(n_x, n_z) = (0, 0)$ are present (for example, the $(0, 0, 1)$ mode may be among the several most important modes). The first four Fourier modes have the same wavenumbers for all three datasets, indicating that these modes capture well the overall behavior of the total duration of the DNS simulation.

The modes given in Table 1 were computed for the full channel. POD modes for a half of the domain can be computed as well.[12] Half-channel modes (from upper wall to centerline) were computed for one of the datasets, resulting in a better energy budget.

Table 2 shows the comparison of the most significant Fourier and traveling modes for the upper half of the channel. Here the first five most significant Fourier modes would give a 13-dimensional dynamical system, and the energy content of the 13 most significant traveling modes is 33.7% higher. Still, for this dataset, 113 Fourier modes or 84 traveling modes were necessary to capture 90% of the energy. A comparison of the POD modes reveals that overall qualitatively similar structures are observed by both traveling and Fourier modes, with the distinction that the traveling modes need only to conform to the symmetry properties of the problem, and not to a particular Fourier wavenumber pair in the streamwise and spanwise directions.

For the purpose of identifying vortical structures in the flow, iso-surfaces of the Q criterion are plotted in figure 1. (The Q criterion[14] is given by $Q = [|\Omega|^2 - |S|^2]/2$, where $\Omega$ and $S$ are respectively the anti-symmetric (vorticity) and symmetric (rate of strain) components of the velocity gradient tensor. Figure 1 indicates a pair of streamwise vortices near each wall (the mode is symmetric as imposed by the symmetrization mentioned

**Table 2. Comparison of the energy budget for Fourier and traveling modes for upper half of the channel**

| 'ranking' | $n_x, n_x, n$ (for Fourier modes) | Fourier $\lambda/E$ | traveling $\lambda/E$ |
|---|---|---|---|
| 1 | $1, \pm 1, 1$ | 0.242 | 0.177 |
| 2 | $\pm 1, \pm 1, 1$ | 0.099 | 0.103 |
| 3 | $0, \pm 1, 2$ | 0.043 | 0.055 |
| 4 | $0, 0, 1$ | 0.031 | 0.043 |
| 5 | $\pm 1, \pm 1, 2$ | 0.030 | 0.042 |
| total | | 0.445 | 0.420 |
| 13 modes | | | 0.595 |

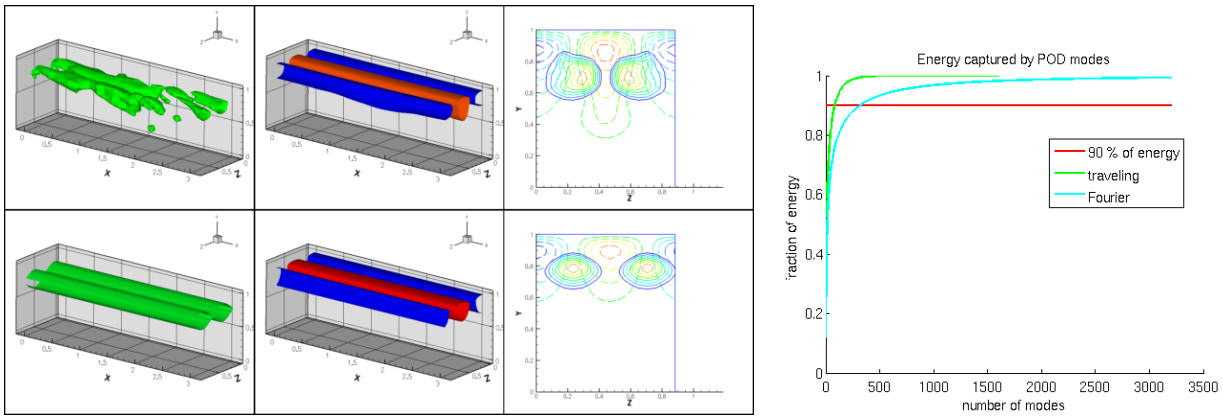


**Figure 1. The $(0, 1, 1)$ Fourier mode (bottom) and the most significant traveling mode (top) for the upper half of the channel. The figure shows iso-surfaces of the Q-criterion (left), streamwise velocity (middle; red color is positive and blue is negative) and a $y, z$ cross-section (right; dotted line is streamwise velocity and solid line is Q-criterion). The figure on the right is a comparison of the energy captured by the traveling and standard POD modes.**

above), approximately in the region $y^+ \approx 20$–$50$, which was also observed by Jimenez and Moin as the dominating structure.[10]

As seen above, fewer modes are needed to capture the energy in the flow using traveling POD. In addition, using the Fourier mode method, a set of $4m$ modes is obtained for each wavenumber, while there are only $4m$ traveling modes (the factor of four is due to the symmetrization mentioned above). Still, turbulence in the minimal unit exhibits rich behavior at all wavenumbers, and although more than half of the energy is captured by the first several modes, a true high-fidelity model would have to be high-dimensional.

# III. Transitional channel flow

## A. Balanced Truncation and Balanced POD

A related problem where reduced-order models can be developed successfully is that of transitional channel flow, in which a stable laminar profile is perturbed, and transients grow large due to non-normality of the linearized operator.[15–17] Here we are interested in delaying transition, rather than controlling or re-laminarizing an already turbulent flow such as the MFU. For these reduced order models, we use an approximation of balanced truncation, a model reduction method popular in the control theory community for model reduction of linear input-output systems.[18,19] The system is written in the form

$$\begin{aligned} \dot{x} &= Ax + Bu \\ y &= Cx \end{aligned} \tag{5}$$

where $x(t) \in \mathcal{X}$ is the state, $u(t) \in \mathcal{U}$ is the input, and $y(t) \in \mathcal{Y}$ is the output, and $\mathcal{X}$, $\mathcal{U}$, and $\mathcal{Y}$ are Hilbert spaces. Since we are interested in models that capture the behavior of the whole fluid flow, we will take $y = x$, but for reasons that will be explained, we will use different inner products on the spaces $\mathcal{X}$ and $\mathcal{Y}$. If the system is both controllable and observable, one can determine a coordinate system in which the controllability and observability Gramians, defined respectively by

$$W_c = \int_0^\infty e^{At} B B^* e^{A^* t}\, dt, \quad W_o = \int_0^\infty e^{A^* t} C^* C e^{At}\, dt, \tag{6}$$

are equal and diagonal (equal to the matrix of Hankel singular values). If the system (5) is written in these coordinates, it is known as a *balanced realization*. One then truncates the states that are least controllable and observable, corresponding to the smallest Hankel singular values.[18,20] This procedure results in low-order models whose stability is guaranteed in most cases (see Sec. III.C), and which have low error bounds.

The required Gramians are usually computed by solving Lyapunov equations. However, this computation is not tractable for very large systems, say with state dimension $n > 10^4$, as the Gramians are non-sparse $n \times n$ matrices. For large systems, a computationally more efficient way is to compute the Gramians empirically using data from simulations, much as POD modes are constructed,[21] and then compute the needed coordinate transformation using the *method of snapshots*.[11] The empirical controllability Gramian is constructed by computing the response $x(t)$ to an impulsive input, forming a matrix $X$ whose columns are snapshots of the state vector ($x(t_j)$ for various times $t_j$), weighted appropriately by quadrature coefficients, so that the matrix product $W_c = XX^*$ approximates the controllability Gramian. For the observability Gramian, we need impulse-state responses of the adjoint system

$$\dot{z} = A^* z + C^* v, \qquad v \in \mathcal{Y} \tag{7}$$

with $z(0) = 0$ and impulses on each component of $v$. Here $A^* : \mathcal{X} \to \mathcal{X}$ is the adjoint of $A : \mathcal{X} \to \mathcal{X}$ and $C^* : \mathcal{Y} \to \mathcal{X}$ is the adjoint of $C : \mathcal{X} \to \mathcal{Y}$. The Gramian is then approximated by $W_o = YY^*$ where the matrix $Y$ is composed of the snapshots of the adjoint simulations. If the number of outputs is large, as in our case where $y = x$, then this method is intractable, since the number of required adjoint simulations is the same as the number of the states of the system. However, an output projection method was introduced by Rowley,[11] in which one first projects the output $y$ onto POD modes of the impulse response, obtaining an input-output system that is the same order as the original system (no Galerkin projection is performed), but with a much smaller dimensional output. For this new system, the computation of adjoint simulations and empirical observability Gramians is then tractable, since the number of adjoint simulations needed is the dimension of the output projection.

Once the data from the primal and adjoint simulations is obtained, one computes the singular value decomposition

$$Y^*X = U\Sigma V^*, \tag{8}$$

where $\Sigma \in \mathbb{R}^{p\times p}$ is the diagonal matrix of nonzero Hankel singular values, and $U \in \mathbb{R}^{l\times p}$ and $V \in \mathbb{R}^{m\times p}$ satisfy $U^*U = V^*V = I_p$. The balancing transformation is then found by computing matrices

$$T = XV\Sigma^{-1/2}, \quad S = \Sigma^{-1/2}U^*Y^* \tag{9}$$

where columns of $T$ are *primal modes* $\varphi_j$, analogous to POD modes, and columns of $S^*$ are *dual modes* $\psi_j$. For this method, the primal and dual modes satisfy a bi-orthogonality relationship $\langle \psi_j, \varphi_k \rangle = \delta_{jk}$.

Knowing both $S$ and $T$, one may obtain balanced truncations directly, without literally transforming the entire state to new coordinates (which would be computationally expensive for systems of this order) and subsequently truncating. If $q$ is the desired order of the reduced-order model, one lets $T_1$ denote the first $q$ columns of $T$, and $S_1$ the first $q$ rows of $S$, and then the reduced-order model is given by

$$\begin{aligned} \dot{z} &= S_1AT_1z + S_1B \\ y &= CT_1z \end{aligned}$$

Note, however, that this is not equivalent to orthogonal projection onto the first $q$ columns of $T$, since these columns are not orthogonal with respect to the standard inner product. (Instead, the columns of $T$ and the rows of $S$ form a bi-orthogonal set.[11])

### B. Linearized Channel Flow

For this geometry, the linearized equations may be conveniently written in terms of the wall-normal velocity $v$ and the wall-normal vorticity $\eta$.[22] The streamwise and spanwise velocities $u$ and $w$ may then be computed using the continuity equation $\partial_x u + \partial_y v + \partial_z w = 0$. In these coordinates, the linearized (nondimensional) equations have the form

$$\frac{\partial}{\partial t}\begin{bmatrix} -\Delta & 0 \\ 0 & I \end{bmatrix}\begin{bmatrix} v \\ \eta \end{bmatrix} = \begin{bmatrix} L_{OS} & 0 \\ -U'\partial_z & L_{SQ} \end{bmatrix}\begin{bmatrix} v \\ \eta \end{bmatrix} \tag{10}$$

where $\Delta = \partial_x^2 + \partial_y^2 + \partial_z^2$ is the Laplacian, and

$$\begin{aligned} L_{OS} &= U\partial_x\Delta - U''\partial_x - \frac{1}{R}\Delta^2 \\ L_{SQ} &= -U\partial_x + \frac{1}{R}\Delta \end{aligned}$$

are the Orr-Sommerfeld and Squire operators, respectively. Here, $R = U_{cl}\delta/\nu$ is the Reynolds number, where $\nu$ is the kinematic viscosity. We will define the operator $M : \mathcal{X} \to \mathcal{X}$ as

$$M = \begin{bmatrix} -\Delta & 0 \\ 0 & I \end{bmatrix} \tag{11}$$

The adjoint system is defined with respect to a suitable inner product on the vector space $\mathcal{X}$ of flow variables $(v, \eta)$. We define the inner product

$$\langle (v_1, \eta_1), (v_2, \eta_2) \rangle = \int_\Omega (-v_1\Delta v_2 + \eta_1\eta_2)\, dx\, dy\, dz,$$

where $\Omega$ denotes the fluid volume. Note that this is just the $L_2$ inner product of $(v_1, \eta_1)$ with $M(v_2, \eta_2)$. Having defined this inner product, we find the adjoint operator via integration by parts:

$$\frac{\partial}{\partial t}\begin{bmatrix} -\Delta & 0 \\ 0 & I \end{bmatrix}\begin{bmatrix} v \\ \eta \end{bmatrix} = \begin{bmatrix} L_{OS}^* & U'\partial_z \\ 0 & L_{SQ}^* \end{bmatrix}\begin{bmatrix} v \\ \eta \end{bmatrix} \tag{12}$$

where

$$\begin{aligned} L_{OS}^* &= -U\partial_x\Delta - 2U'\partial_x\partial_y - \frac{1}{R}\Delta^2 \\ L_{SQ}^* &= U\partial_x + \frac{1}{R}\Delta. \end{aligned}$$

### C. Results

Previous work has applied the balanced POD method to a linearized channel flow with streamwise-constant perturbations, for which full balanced truncation is still tractable, and it was shown that for this case balanced POD is indeed a very accurate approximation to exact balanced truncation and that the resulting models outperform significantly standard POD models.[11] Here we report recent results for three-dimensional peturbations, where full balanced truncation would be intractable.

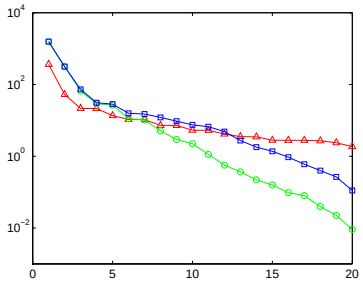


**Figure 2. The first 20 POD eigenvalues (△) and Hankel singular values for four-mode (○) and nine-mode (□) output projections at $Re = 1000$.**

The forward simulations were performed for a Gaussian-like disturbance in the center of the channel at centerline Reynolds number $Re = 1000$. A modification of the numerical simulation described in Sec. II.B was used, in which the solver was modified for the linearized (forward and adjoint) equations. The grid size was $32 \times 33 \times 16$, corresponding to 33,792 states for the full $(v, \eta)$ system. The simulation was run until $t = 1000$, where $t = t^d U_{cl}/\delta$, and the timestep used was $\Delta t = 0.004$. During this time, the $L_2$ norm of the initial disturbance decayed to 1 percent of its initial value. The POD modes were taken over 1000 snapshots, with spacing between snapshots of 1 time unit, after it was verified that POD eigenvalues for a higher number of snapshots do not change significantly. Fig. 2 shows the POD eigenvalues of the forward simulation and the Hankel singular values of the product $Y^*X$. The choice for the rank of the output projection was made based on the energy content in the POD modes: the first four modes contain 82.21% of the energy and the first nine modes contain 91.05% of the energy.

The first four standard POD modes are shown in Fig. 3. The first two modes are streamwise-constant structures, while the third and the fourth mode have a fully three-dimensional structure. It is interesting to note that the eigenvalues in Fig. 2 corresponding to the third and fourth modes are equal, as well as for the pairs 6–7 and 8–9. These modes typically come in pairs 90° out of phase, representing traveling structures, just as sin and cos functions can represent one-dimensional traveling waves.

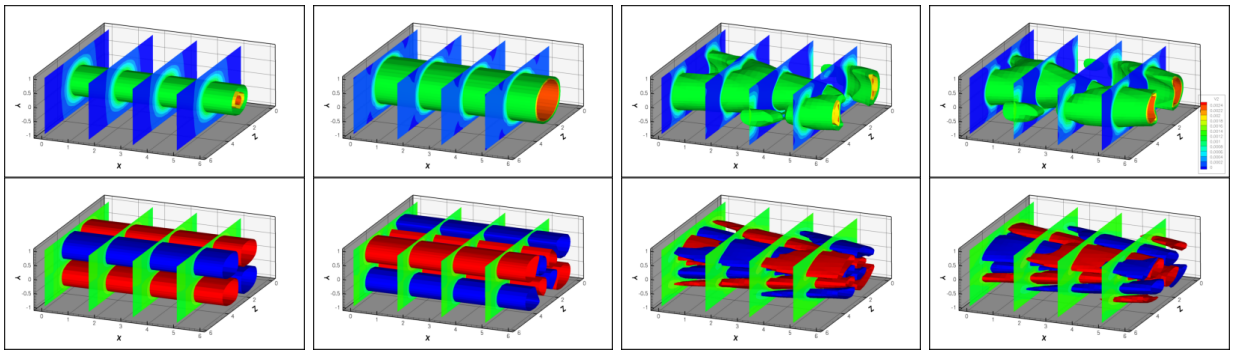

**Figure 3. First four standard POD modes, showing wall-normal velocity $v$ (top) and vorticity $\eta$ (bottom).**

Adjoint simulations were performed for the first nine modes, and low-order models were formed for output projection ranks 4 and 9. Balanced POD modes one, two, four, and five, and the corresponding adjoint modes for the nine-mode output projection are shown in Fig. 4. In Fig. 2, the Hankel singular values 4–5 and 6–7 for both 4-mode and 9-mode output projection appear to be approximately equal, corresponding

to out-of-phase pairs of modes. It was observed that 4-mode and 6-mode models for both output projections are unstable, indicating that both modes in each pair should always be kept for a stable low-order model. (While generically, balanced truncations are guaranteed to be stable, it is known that this holds only in the case when $\sigma_{r+1} < \sigma_r$, where $r$ is the number of states retained.[20]) Note that the structure of modes four and five in Fig. 4 is almost identical, except for a spatial phase shift of exactly one quarter of the periodic domain.

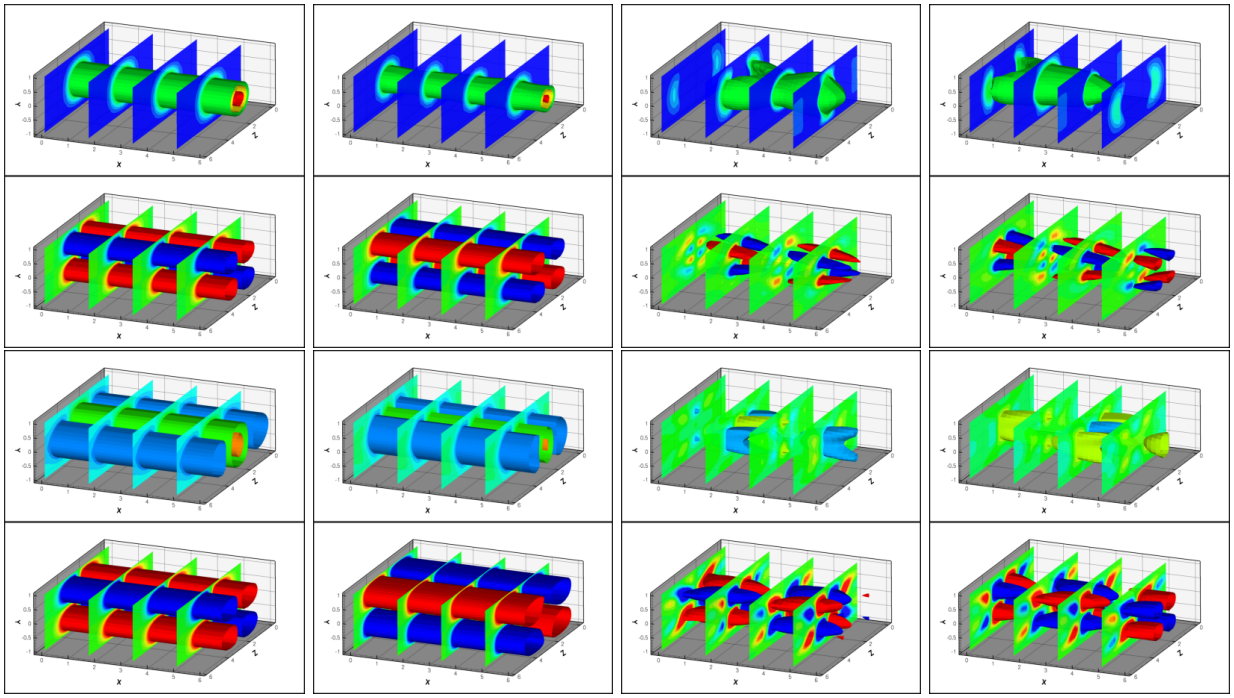

**Figure 4. Top two rows: primal modes one, two, four and five from balanced POD, showing wall-normal velocity $v$ (top) and vorticity $\eta$ (bottom). Bottom two rows: the corresponding adjoint modes. Note the similarity between the primal modes and the corresponding POD modes in Fig. 3.**

Simulations of various reduced-order models are shown in Figure 5, which compares an 8-mode balanced POD model (9-mode output projection) with 8-mode and 29-mode standard POD models, as well as the projection of the full simulation onto the POD modes. The coefficients of the first three POD modes are shown for all simulations: note that for the balanced POD model, these are not the actual states in the model, but they are the first three outputs defined by the output projection procedure described in Sec. A.

### D. Projection of input onto the subspace

In order for a reduced-order model to capture the effect of an actuator, it is necessary at a minimum for the input term in the equations ($Bu$ in (5)) to be contained in the subspace used for projecting the equations. One way to measure the degree to which the input "directions" are captured by the modes used in the model is to compute the projection of the columns of the input matrix $B$ in (5) onto the basis modes. In the system considered here, $B$ is a single column vector, representing the initial disturbance given to the system (or actuation via a body force in the center of the domain). Fig. 6 shows the norm of the projection $\|P_r B\|/\|B\|$ of the standard and balanced POD modes onto the input vector $B$ for the cases of $Re = 100$ (this simulation was done at a smaller grid, $16 \times 17 \times 16$ and until $t = 200$) and $Re = 1000$. Clearly, for the $Re = 1000$ case, the $B$ matrix has a very small projection onto the POD modes for standard POD unless many modes are taken, so it is impossible for very low-order POD models to capture the response of an actuator without introducing more modes (such as the $B$ matrix itself, Krylov subspaces, or shift modes[5]). Note that here, even for the standard POD case, the effect of the "actuator" is partially included, since the dataset used for POD is generated by an impulsive input. For $Re = 100$ the dynamics are simpler, and the behavior of POD subspaces becomes reasonably good at the order of several modes.

The balanced POD modes clearly capture the input direction with many fewer modes than standard

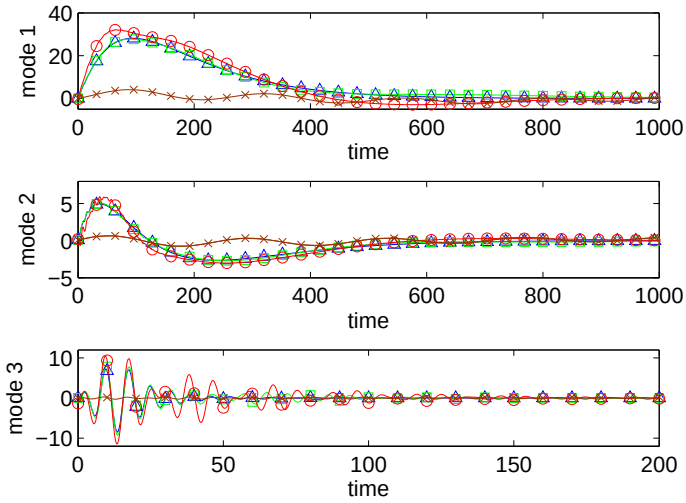


**Figure 5. Impulse response for $Re = 1000$ case: time coefficients of first three POD modes of different reduced-order models. 8-mode balanced POD (○); 8-mode standard POD (×); 29-mode standard POD (△), and projection of the full simulation (—). The 29-mode model almost perfectly reproduces the full simulation, but 8-mode balanced POD is much more accurate than 8-mode standard POD.**

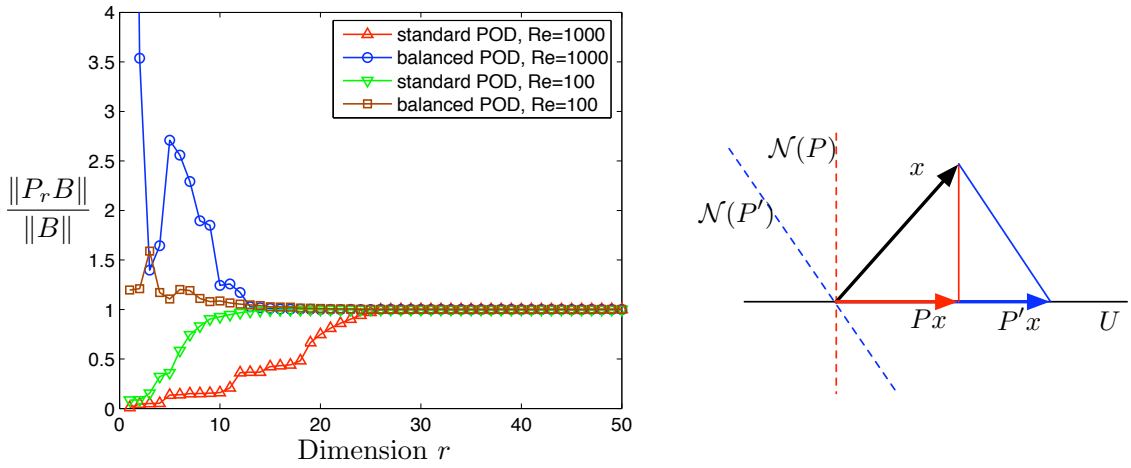


**Figure 6. Left: norm of the projection of the $B$ matrix (a single column vector) onto subspaces used for reduced-order models, as a function of the dimension of the subspace, for both $Re = 100$ and $Re = 1000$ cases, showing standard POD (▽, △), and balanced POD (□, ◯). Right: diagram illustrating that for a non-orthogonal projection such as used with balanced POD, the norm of a vector can increase after projection. Here, $P$ and $P'$ are projections onto a subspace $U$, with nullspaces indicated by the dashed lines. Note that any orthogonal projection such as $P$ must satisfy $\|Px\| \leq \|x\|$, while for a non-orthogonal projection we may have $\|P'x\| > \|x\|$.**

POD: even very low-order models have a significant norm after projection, and in fact the norm of $B$ after projection is always greater than the norm of $B$ before projection. This may seem surprising at first, since the (primal) modes themselves are quite similar between standard and balanced POD (compare Figs. 3 and 4). It is in fact the adjoint modes, or equivalently, the definition of the inner product used for the projection, that makes the biggest difference here. See Fig. 6 (right) for a geometric explanation of the significance of different projections. Of course, merely checking that the input direction is retained after projection does not guarantee that the dynamics will be accurately described, so we explore that question next.

### E. Response to a sinusoidal input

The response of the low-order models to sinusoidal inputs was compared for both standard and balanced POD models. The same localized disturbance in the center of the channel which was used as an initial condition to obtain the impulse response of the system was forced with a unit amplitude sinusoidal input at a range of frequencies. The low-order models obtained from the impulse response were then forced at these frequencies. Fig. 7 shows the response of the first three modes of a 8-mode balanced POD model at the dimensionless frequency of $\omega = 0.33$, compared to the results of the 8-mode and 29-mode POD models whose impulse responses were shown in Fig. 5. The balanced POD model shown is from a 9-mode output projection, however, even for a 4-mode output projection, change in the model performance was not appreciable, which is interesting since the effect on the impulse response is quite significant as seen in Fig. 5. The standard POD model does not capture the oscillation at all, even though the model is of a fairly high dimension.

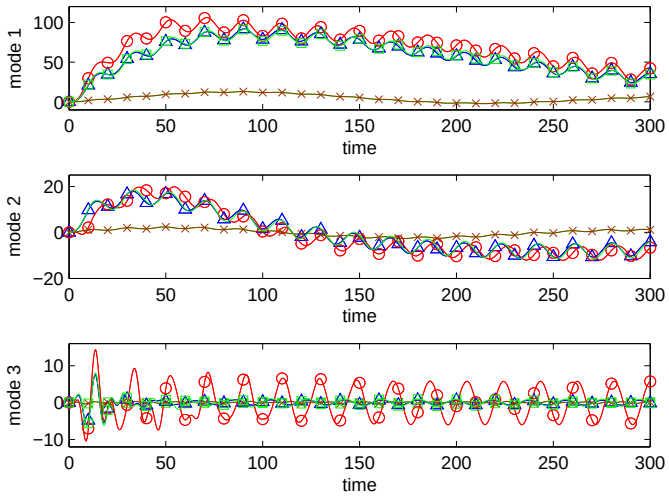


**Figure 7. Sinusoidal forcing for $Re = 1000$: First three modes with forcing $u = \sin \omega t$ with $\omega = 0.33$, for various reduced-order models: 8-mode balanced POD (○); 8-mode standard POD (×); 29-mode standard POD (△), and projection of the full simulation (—). As with the impulse response, the 29-mode model almost perfectly reproduces the full simulation, but 8-mode balanced POD is much more accurate than 8-mode standard POD, which does not respond at all to the forcing.**

## IV. Conclusions

Reduced-order models for flow in a plane channel have been investigated in two different regimes. First, empirical basis functions were computed for the turbulent flow in a minimal flow unit channel, using the standard POD procedure, and comparing with traveling POD modes. The traveling modes captured a greater fraction of the energy, for a fixed dimension of the projection, but nevertheless a large number of modes was required to capture 90% of the energy in the fluctuations (84 for traveling POD, 113 for standard POD), indicating that very low-order models that accurately capture the details of the dynamics of the turbulent flow in this regime are probably not feasible.

In a study of a different regime, linearized flow about a laminar profile, it was shown that accurate

low-dimensional models can be obtained using the balanced POD method, an approximation of balanced truncation that is tractable for very large systems. As indicated by the response to impulsive and sinusoidal inputs, balanced POD was shown to significantly outperform standard POD, and relatively small models (8 modes) can accurately capture the dynamics of the flow. Future directions of this work include using balanced POD to obtain accurate models of realistic transition mechanisms and adding physically realizable actuation mechanisms for closed-loop control systems.

This work was supported by the National Science Foundation, award CMS-0347239.

## References

[1]Lumley, J. L., *Stochastic Tools in Turbulence*, Academic Press, New York, 1970.

[2]Holmes, P., Lumley, J., and Berkooz, G., *Turbulence, Coherent structures, Dynamical Systems and Symmetry*, Cambridge University Press, 1996.

[3]Sirovich, L., "Turbulence and the dynamics of coherent structures, pt. I-III," *Quarterly of Applied Mathematics*, 1987.

[4]Smith, T., *Low-dimensional models of plane Couette flow using the Proper Orthogonal Decomposition*, Ph.D. thesis, Princeton University, 2003.

[5]Noack, B., Afanasiev, K., Morzyński, M., Tadmor, G., and Thiele, F., "A hierarchy of low-dimensional models for the transient and post-transient cylinder wake," *J. Fluid Mech.*, Vol. 497, 2003, pp. 335–363.

[6]Tadmor, G., Noack, B., Morzyński, M., and Siegel, S., "Low-dimensional models for feedback flow control. Part II: Controller design and dynamic estimation," *2nd AIAA Flow Control Conference*, Portland, Oregon, U.S.A., June 28 – July 1, 2004, AIAA Paper 2004-2409 (invited contribution).

[7]Noack, B. R., Papas, P., and Monkewitz, P. A., "The need for a pressure-term representation in empirical Galerkin models of incompressible shear flow," *J. Fluid Mech.*, Vol. 523, 2005, pp. 339–365.

[8]Rowley, C., Colonius, T., and Murray, R., "Model reduction for compressible flows using POD and Galerkin projection," *Physica D*, 2004.

[9]Rowley, C. and Marsden, J., "Reconstruction equations and the Karhunen-Loeve expansion for systems with symmetry," *Physica D*, 2000.

[10]Jimenez, J. and Moin, P., "The minimal flow unit in near-wall turbulence," *J. Fluid Mech.*, 1991.

[11]Rowley, C., "Model reduction for fluids, using balanced proper orthogonal decomposition," *Int. J. on Bifurcation and Chaos*, 2005.

[12]Moin, P. and Moser, R., "Characteristic-eddy decomposition of turbulence in a channel," *J. Fluid Mech.*, 1989.

[13]Kim, J., Moin, P., and Moser, R., "Turbulent statistics in fully developed channel flow at low Reynolds number," *J. Fluid Mech.*, 1987.

[14]Haller, G., "An objective definition of a vortex," *J.Fluid Mech.*, 2005.

[15]Trefethen, L. N., Trefethen, A. E., Reddy, S. C., and Driscoll, T. A., "Hydrodynamic Stability Without Eigenvalues," *Science*, Vol. 261, July 1993, pp. 578–584.

[16]Bamieh, B. and Daleh, M., "Energy amplification in channel flows with stochastic excitation," *Phys. Fluids*, Vol. 13, No. 11, Nov. 2001, pp. 3258–3269.

[17]Farrell, B. and Ioannou, P., "Accurate low-dimensional approximation of the linear dynamics of fluid flow," *J. Atmos. Sci.*, 2001.

[18]Moore, B. C., "Principal Component Analysis in Linear Systems: Controllability, Observability, and Model Reduction," *IEEE Trans. Automat. Contr.*, Vol. 26, No. 1, Feb. 1981, pp. 17–32.

[19]Cortelezzi, L. and Speyer, J. L., "Robust reduced-order controller of laminar boundary layer transitions," *Phys. Rev. E*, Vol. 58, No. 2, 1998, pp. 1906–1910.

[20]Dullerud, P. and Paganini, F., *A Course in Robust Control Theory: a Robust Approach*, Springer-Verlag, 2000.

[21]Lall, S., Marsden, J., and Glavaski, S., "A subspace approach to balanced truncation for model reduction of nonlinear control systems," *Int. J. Robust Nonlin. Contr.*, 2002.

[22]Schmid, P. and Henningson, D., *Stability and Transition in Shear Flows*, Springer-Verlag, 2001.